resistance in human ovarian carcinoma cells. *BMC Cancer* 2008;8:175.
43. Al-Bahlani S, Fraser M, Wong AY, et al. P73 regulates cisplatin-induced apoptosis in ovarian cancer cells via a calcium/calpain-dependent mechanism. *Oncogene* 2011;30:4219–30.
44. Splettstoesser F, Florea AM, Busselberg D. IP(3) receptor antagonist, 2-APB, attenuates cisplatin induced Ca2+-influx in HeLa-S3 cells and prevents activation of calpain and induction of apoptosis. *Br J Pharmacol* 2007;151: 1176–86.
45. Choi CH, Sung CO, Kim HJ, et al. Overexpression of annexin A4 is associated with chemoresistance in papillary serous adenocarcinoma of the ovary. *Hum Pathol* 2013;44:1017–23.
46. Yan X, Yin J, Yao H, et al. Increased expression of annexin A3 is a mechanism of platinum resistance in ovarian cancer. *Cancer Res* 2010;70:1616–24.
47. Yin J, Yan X, Yao X, et al. Secretion of annexin A3 from ovarian cancer cells and its association with platinum resistance in ovarian cancer patients. *J Cell Mol Med* 2012;16:337–48.

JVI
Journals.ASM.org

Varicella-Zoster Virus ORF49 Functions in the Efficient Production of Progeny Virus through Its Interaction with Essential Tegument Protein ORF44

Tomohiko Sadaoka,[a,b] Satoshi Serada,[c] Junko Kato,[a] Mayuko Hayashi,[a,b] Yasuyuki Gomi,[d] Tetsuji Naka,[c] Koichi Yamanishi,[e] Yasuko Mori[a,b]

Division of Clinical Virology, Center for Infectious Diseases, Kobe University Graduate School of Medicine, Kusunoki-cho, Chuo-ku, Kobe, Japan[a]; Laboratory of Virology and Vaccinology, Division of Biomedical Research, National Institute of Biomedical Innovation, Saito-Asagi, Ibaraki, Osaka, Japan[b]; Laboratory of Immune Signal, Division of Biomedical Research, National Institute of Biomedical Innovation, Saito-Asagi, Ibaraki, Osaka, Japan[c]; Kanonji Institute, The Research Foundation for Microbial Diseases of Osaka University, Kanonji, Kagawa, Japan[d]; National Institute of Biomedical Innovation, Saito-Asagi, Ibaraki, Osaka, Japan[e]

The ORF49 tegument protein of varicella-zoster virus (VZV) is one of the core gene products that is conserved among herpesvirus family members. Although ORF49 is known to be a cell-tropic factor, its detailed functions remain elusive. ORF44 is another core gene product reported to be essential, although its characterization and detailed functional analysis have not been reported. These two core gene products form a complex in other herpesviruses beyond the host species and herpesvirus subfamilies. Here, we show that complex formation between ORF44 and ORF49 is conserved in VZV. We serendipitously found that binding is eliminated by an amino acid substitution at position 129 (phenylalanine 129), and four amino acids in the carboxyl-terminal half of the acidic cluster in ORF49 (i.e., aspartate-phenylalanine-aspartate-glutamate from positions 41 to 44 [41DFDE44]) were identified as its binding motif. Alanine substitutions in each domain rendered the ORF44F129A mutation lethal for VZV, similar to deletion of the entire ORF44. The phenotype of the ORF49-41AAAA44 mutation was comparable to that of the ORF49-defective virus, including small-plaque formation, impaired growth, and low infectious virus production. These results suggest that the interaction between ORF44 and ORF49 is essential for their role in VZV infection and that ORF49 is required for the efficient production of infectious progeny virus mediated by the conserved interaction between the two proteins.

Varicella-zoster virus (VZV) is a member of the human alphaherpesvirus subfamily and the etiologic agent of two diseases: varicella is the result of primary infection with VZV, and herpes-zoster is caused by reactivation of the virus from the latent state (1). VZV shares many features, especially a tropism for epithelial and neural tissues, with other human alphaherpesvirus members, including herpes simplex viruses 1 and 2 (HSV-1 and -2, respectively), and with the nonhuman alphaherpesviruses. However, VZV spreads only via cell-to-cell infection in culture and is more akin to the betaherpesviruses (i.e., human herpesviruses 6 and 7) in its apparent T-cell-tropism (1).

The VZV genome is approximately 125 kb and contains at least 70 unique open reading frames (ORFs), and it is the smallest genome in terms of length and gene set among human herpesviruses (1–3). Of the 70 identified ORFs, 44 are core genes that are conserved among all human herpesvirus subfamilies (4). Recent genome-wide mutagenesis analysis showed that 34 ORFs among the core genes are essential for virus reconstitution in cell culture, whereas deletion of seven ORFs results in viral growth defects, and three ORFs are dispensable in cell culture or skin organ culture (5). Eight core genes encode tegument proteins, which are the structural components of the virion and are located between the nucleocapsid and the envelope.

VZV ORF49 encodes a nonessential tegument protein that functions as a cell-tropic factor in cell culture via an unknown mechanism (6). VZV ORF49 is the homolog of HSV-1 UL11 and human cytomegalovirus (HCMV) UL99, which are among the most extensively studied tegument protein-encoding genes. The UL11 and UL99 gene products, pUL11 and pp28, function in secondary envelopment (7–9), but they have different roles in the viral life cycle. HSV-1 UL11 is not essential for the viral life cycle; however, the UL11 deletion mutant forms small plaques, and the final titers are reduced to 80 to 95% of wild-type levels (10). In contrast, HCMV UL99 is an essential gene, and pp28-deficient mutants show extremely impaired growth in normal fibroblasts and produce no detectable infectious progeny (9). However, this mutant spreads from cell to cell via an unknown mechanism (11).

Several recent reports, beginning with one on HSV-1 UL16, which is a core gene within the intron of a conserved herpesvirus spliced gene, (12), showed that interactions between pUL11 and pUL16 homologs were conserved beyond the host species and herpesvirus subfamilies (13–15). HSV pUL16 localizes to the nucleus and the cytoplasm of infected cells and functions in virus entry and in nuclear and cytoplasmic egress (16–19); pUL16 homologs may function in secondary envelopment, as reviewed in reference 20. As described for UL11 homologs, whether UL16 homologs are required for the viral life cycle differs among viruses (13, 15, 21–25). In a genome-wide mutagenesis analysis, deletion of the entire gene region from the viral genome of VZV ORF44, the UL16 homolog, showed that it is an essential gene by loss-of-function analysis in the MeWo cell line (5), although this was not

Received 11 August 2013 **Accepted** 10 October 2013
Published ahead of print 23 October 2013
Address correspondence to Yasuko Mori, ymori@med.kobe-u.ac.jp.

doi:10.1128/JVI.02245-13

confirmed by a revertant virus generated for gain-of-function analysis.

The LI motif and the conserved acidic cluster of pUL11 are essential for its interaction with pUL16 of HSV-1, whereas the critical sequences in pUL16 have not been determined because it is highly sensitive to deletions. Its short N-terminal 75-amino-acid (aa) fragment was recently shown to include the pUL11 binding site, and its C-terminal region functions as the binding regulatory domain (26), although this has not been confirmed in the context of HSV-1-infection. HCMV pUL94 directs pp28 to the assembly compartment, where it plays a role in secondary envelopment. Amino acids 37 to 39, near the acidic cluster of pp28, and one of the conserved cysteine residues of pUL94 are involved in binding in the context of infection (24, 27). In VZV, potential ORF49 protein (ORF49p)-binding proteins, including the pUL16 homolog ORF44 protein (ORF44p), were identified by global screening using the yeast two-hybrid system (28, 29), although these interactions have not been confirmed, even by coexpression experiments in mammalian cells.

In our previous study on VZV ORF49 (6), ORF49p was identified as one of the cell-tropic factors for VZV lytic infection in cell culture. However, the precise function of ORF49 in cells in which the ORF49-defective virus showed impaired growth was not elucidated. To address this issue, we established a complete *trans*-complementation system for ORF49 and identified ORF44p as its binding partner in the context of infection. In the present study, we aimed to reveal the precise role of ORF49p by using this system and by analyzing the conserved mechanism of interaction between these proteins and its role in VZV infection.

MATERIALS AND METHODS

Cells and viruses. The melanoma cell line MeWo was propagated in Dulbecco's modified Eagle's medium (DMEM) (Nissui Pharmaceutical, Ueno, Tokyo) supplemented with 8% fetal bovine serum (FBS) (Sigma-Aldrich, St. Louis, MO), 0.6 mg/ml L-sodium glutamate, and 0.02 mg/ml gentamicin sulfate (Nacalai Tesque, Kyoto, Japan) (DMEM complete). MeWo cells stably expressing Cre recombinase, designated MeWo-Cre cells, were maintained in DMEM complete supplemented with 500 μg/ml G418 (Nacalai Tesque) (30). MeWoORF49 cells stably expressing ORF49 were generated as follows: MeWo cells were transfected with CAG/ORF49 (described below) using Lipofectamine 2000 (Invitrogen, Carlsbad, CA) according to the manufacturer's instructions, selected, and propagated in DMEM complete supplemented with 1.5 μg/ml puromycin (Invitrogen). Recombinant viruses derived from the parental VZV strain Oka (pOka), rpOka, rpOkaΔ44Rev, rpOkaORF44F129ARev, rpOkaORF44T128A, rpOkaORF44K130A, rpOkaORF49M1L, rpOkaORF49M1LRev, rpOka-ORF49-41AAAA44, and rpOkaORF49-41AAAA44Rev were maintained in DMEM complete supplemented with 3% FBS.

Cell-free virus was prepared as described previously with slight modifications (6). At 48 h postinfection (hpi) by cell-to-cell spread, cells were harvested with a cell scraper (Iwaki, Tokyo, Japan), spun at 800 × *g* for 5 min at 4°C, and suspended in SGP buffer (phosphate-buffered saline [PBS] containing 0.1% L-sodium glutamate and 7% sucrose). The suspended cells were treated with an ultrasonic disruptor (UD-201; Tomy Seiko, Tokyo, Japan) at 1.5° for 30 s on ice and spun at 800 × *g* for 5 min at 4°C, and the supernatant was stored at −80°C until use. The purified viral particles were prepared as described in reference 6. Briefly, the cell-free virus solutions were subjected to Histodenz (Sigma-Aldrich) gradient purification (5 to 50% in PBS) by ultracentrifugation at 50,200 × *g* for 2 h at 4°C in a P40ST rotor (CP80WX; Hitachi Koki, Hitachinaka, Japan). Aliquots of the peak particle-containing fractions were subjected to ultracentrifugation at 52,600 × *g* for 2 h at 4°C in a P28S rotor (CP80WX; Hitachi Koki), and the pellets were stored at −80°C for further analyses.

Plasmids. The pGEX/ORF44, pGEX/ORF44A, and pGEX/ORF44P plasmids were generated to express the full length (corresponding to aa 2 to 363), anterior half (aa 2 to 200), and posterior half (aa 181 to 363) of the ORF44 protein in *Escherichia coli*. The primer pairs ORF44ecoF4 (5′-ACCGAATTCGAATTACAACGCATATTTCCG-3′) and ORF44salR (5′-ACCGTCGACCTAGGTGGTTGTAGG-3′) for ORF44, ORF44ecoF4 and ORF44salR600 (5′-ACCGTCGACTAAATTAGGTTCCATAGCC-3′) for ORF44A, and ORF44ecoF541 (5′-ACCGAATTCGGAGTGTGGTGGTCAGACG-3′) and ORF44salR for ORF44P were used to amplify each indicated region of the ORF44 gene from the rpOka cDNA. The PCR products were inserted in frame into the pGEX6P-1 bacterial expression vector (GE Healthcare Bio-Sciences, Piscataway, NJ) via the EcoRI and SalI sites (underlined). The same procedure was used to construct pGEX/ORF61. The DNA fragment (positions 406 to 744) of ORF61 was cloned into pGEX6P-1 via the BamHI and SalI sites (underlined). The primer pair was ORF61bamF406 (5′-ACCGGATCCGGGCCCCTTCAATCGTCGG-3′) and ORF61salR744stop (5′-ACCGTCGACCTAGAATCTCGCGTTTCCCTC-3′). The eukaryotic ORF44 expression plasmid CAG/ORF44 or CAG/FLAGORF44, which was N-terminally tagged with FLAG (DYKDDDDK), was generated as follows: the entire ORF44 gene was amplified by PCR with the primers ORF44-25kpnF (5′-ACCGGTACCAATCCGCTAGACTG-3′) or ORF44FLAGkpnF4 (5′-ACCGGTACCGCCACCATGgactacaaagacgatgacgacaagGAATTACAACGCATATTTCCG-3′) and ORF44salR, and the PCR fragment was cut by KpnI and SalI (underlined) and cloned into pCAGGS-MCS-neo via the KpnI and XhoI sites. The FLAG tag coding sequence within the primer for ORF44FLAGkpnF4 is shown in lowercase letters. The ORF49 expression plasmid CAG/ORF49 was generated as follows: the entire ORF49 gene was amplified by PCR with the primers ORF49-24ecoF (5′-ACCGAATTCTTACATCAGCATTGCG−3′) and ORF49bamR (5′-ACCGGATCCTTAACATTTTGCGCATTTGG-3′), and the PCR fragment was cut by EcoRI and BamHI (underlined) and cloned into pCAGGS-MCS-puro via the EcoRI and BglII sites. The pCAGGS plasmid was kindly provided by Jun-ichi Miyazaki (Osaka University, Japan) (31). A Cre recombinase-expressing plasmid, pCX-Cre-neo, was previously generated (30) from pCX-Cre, which was a generous gift from Masaru Okabe (Osaka University, Japan).

Construction of mutant ORF44 and ORF49 expression plasmids. The ORF44 mutant plasmids pGEX/ORF44F129A, CAG/ORF44T128A, CAG/ORF44F129A, CAG/ORF44K130A, CAG/FLAGORF44I121stop, CAG/FLAGORF44P136stop, and CAG/FLAGORF44F129AP136stop and the ORF49 mutant plasmid CAG/ORF49-41AAAA44 were generated with a QuikChange Lightning multisite-directed mutagenesis kit (Agilent Technologies, La Jolla, CA) according to the manufacturer's recommendations, using the primers listed in Table 1 based on pGEX/ORF44, CAG/ORF44, CAG/FLAGORF44, and CAG/ORF49, respectively. The ORF49 C-terminal deletion mutant plasmids CAG/ORF49N40, CAG/ORF49N44, and CAG/ORF49N48 were generated using the following primer pairs: ORF49-24ecoF (5′-ACCGAATTCTTACATCAGCATTGCG-3′) as the forward primer for all the deletion mutants and ORF49mycxhoR120 (5′-ACCCTCGAGcagatcctcttctgagatgagtttttgttcAAAGTCTTCAAAGAACTCTG-3′), ORF49mycxhoR132 (5′-ACCCTCGAGcagatcctcttctgagatgagtttttgttcCTCATCAAAGTCAAAGTCTT-3′), or ORF49mycxhoR144 (5′-ACCCTCGAGcagatcctcttctgagatgag tttttgttcCTCTGTTACATTCTCATCAAAGTC-3′) as the reverse primer for CAG/ORF49N40, CAG/ORF49N44, or CAG/ORF49N48. All of the reverse primers contained a c-myc tag, indicated by lowercase letters, and the PCR products were cloned into pCAGGS-MCS-puro via the EcoRI and XhoI sites (underlined).

Antibodies. To produce a mouse monoclonal antibody (MAb) against ORF44, a glutathione *S*-transferase (GST)-ORF44A recombinant protein was expressed in *E. coli* BL21 transformed with pGEX/ORF44A, purified, and used to immunize mice; hybridoma clones producing the anti-ORF44 MAb were established as described previously (32). To produce polyclonal anti-ORF61 Abs, a GST-ORF61 fusion protein was purified from *E. coli* BL21 transformed with pGEX-ORF61 and used to immunize a rabbit

TABLE 1 Primers used for ORF44 or ORF49 mutations

Primer	Sequence[a]	Amino acid substitution(s)
ORF44 361at-ta	5′-TAT CCG GTT GAA AAC TAA GAC CAT GTT TTT GGA-3′	Ile 121 to stop (TAA)
ORF44 382a-g	5′-CAT GTT TTT GGA GCA GCG TTT AAG AAC CC-3′	Thr 128 to Ala
ORF44 385tt-gc	5′-TT TTT GGA GCA ACG GCT AAG AAC CCG ATC G-3′	Phe 129 to Ala
ORF44 388aa-gc	5′-TTT GGA GCA ACG TTT GCG AAC CCG ATC GCG-3′	Lys 130 to Ala
ORF44 406ccc-taa	5′-AAC CCG ATC GCG TAC TAA CTT CCA ACA TCT ATT-3′	Pro 136 to stop (TAA)
ORF49 M1L	5′-ATT GCG GTC ATT GCG TTG GGA CAA TCT TCA-3′	Met 1 to Leu
ORF49 41AAAA44	5′-TTT GAA GAC TTT GCC GCT GCT GCG AAT GTA ACA GAG-3′	Asp-Phe-Asp-Glu (41–44) to Ala-Ala-Ala-Ala

[a] Nucleotides that differ from those of the wild type are underlined.

(Sigma Genosys, Hokkaido, Japan). The anti-ORF61 Ab was purified with GST-conjugated normal human serum (NHS)-activated Sepharose and GST-ORF61-conjugated NHS-activated Sepharose. Rabbit polyclonal anti-ORF49 and anti-gB-C Abs were described previously (6). The mouse anti-glycoprotein E (anti-gE) (clone 9) Ab was described in reference 33. Mouse anti-glycoprotein H (gH) (VgIII-3) was obtained as described previously (33). Sheep anti-*trans*-Golgi network (anti-TGN46) Ab (AHP500G; AbD Serotec, Oxford, United Kingdom), anti-α-tubulin Ab (B-5-1-2; Sigma-Aldrich), and goat anti-GST Ab (GE Healthcare Bio-Sciences) were commercially available. Alexa Fluor 488-labeled donkey anti-mouse immunoglobulin G (IgG), Alexa Fluor 594-labeled donkey anti-rabbit IgG, and Alexa Fluor 647-labeled donkey anti-sheep IgG (Invitrogen) were used as secondary Abs, and Hoechst 33342 (Sigma-Aldrich) was used for nuclear staining in confocal microscopic analyses. ECL enhanced chemiluminescence anti-mouse or anti-rabbit IgG horseradish peroxidase-linked whole antibodies from donkey (GE Healthcare Bio-Sciences) were used as secondary Abs in immunoblotting.

Mutagenesis of viral genomes in *E. coli*. The mutant bacterial artificial chromosomes (BACs) pOka-BACORF49M1L, containing a methionine-to-leucine substitution at residue Met-1, and pOka-BACORF49-41AAAA44, containing a tetra-alanine substitution at residues 41-Asp-Phe-Asp-Glu-44, were generated by *recA*-mediated allelic replacement in pOka-BAC-harboring DH10B transformed with pST76A-SR/pOkaORF49M1L and pST76A-SR/pOkaORF49-41AAAA44, respectively, which were derived from pST76A-SR/pOkaORF50 (including nucleotide positions 84361 to 89970 of pOka) (30), using the primers listed in Table 1 and a QuikChange Lightning multisite-directed mutagenesis kit. The revertant BACs pOka-BACORF49M1LRev and pOkaBACORF49-41AAAA44Rev were generated by recA-mediated allelic replacement using pST76A-SRORF50 transformed into DH10B cells harboring pOka-BACORF49M1L and pOka-BACORF49-41AAAA44, respectively.

To generate pOka-BACΔ44, in which the nucleotides (nt) 1 to 800 of the ORF44 gene were replaced with an FRT (*flp* recombinase recognition target) sequence, a linear fragment was amplified by PCR using the primer pair ORF44FRTfKMF0 (5′-TTAAACCCACAAGTACC CGGGCGGCAATCCGCTAGACTGTTTTTCTGCTCGAAGTTCCTA TTCTCTAGAAAGTATAGGAACTTCAGCAAGCGAACCGGAAT TGC-3′) and ORF44FRTrKMR800 (5′-TCCCGCTGACCGGCCTTT CTCCACATACACGGAGCCCAACACACACAACCGAAGTTCCTAT ACTTTCTAGAGAATAGGAACTTCCTTTTTCAATTCAGAAGA ACTC-3′) (FRT is underlined) using pCR2.1-TOPO as the template (Invitrogen). The amplified fragment was then transformed into DH10B harboring pOka-BAC (34) with pGETrec (a kind gift from Panayiotis A. Ioannou, The Murdoch Institute for Research into Birth Defects, Royal Children's Hospital, Melbourne, Australia) (35); *recE*/*T* recombination for pOka-BACΔ44KMr and excision of the kanamycin resistance gene from pOka-BACΔ44KMr by the *flp*/FRT system using pCP20 (a kind gift from Wilfried Wackernagel, Universität Oldenburg, Germany) (36), resulting in pOka-BACΔ44, were carried out as described previously (6).

To construct pOka-BACΔ44Rev, the revertant BAC genome against pOka-BACΔ44, *recA*-mediated mutagenesis was performed as described previously (30), using the shuttle plasmid pST76A-SR/pOkaORF44. For pST76A-SR/pOkaORF44, a 3.2-kbp fragment of viral DNA corresponding to nt 79230 to 82453 of pOka was amplified from the pOka-BAC genome using the primer pair ORF43F1201 (5′-ACCGCTGCGTGTATA AATGCCCGGGTTGAC-3′) and ORF42/45F (5′-ACCATGTCATTGAT AATGTTTGG-3′), cloned into pCR2.1-TOPO, sequenced, cut with EcoRI, blunted, and cloned into the plasmid pST76A-SR (kindly provided by Ulrich H. Koszinowski, Max von Pettenkofer Institut, Ludwig-Maximilians-Universität München, Munich, Germany) (37), which was cut with KpnI and blunted.

The shuttle plasmids for the ORF44 point mutant BACs, pST76A-SRORF44T128A (with an alanine substitution for threonine at residue Thr-128), pST76A-SR/pOkaORF44F129A (with an alanine substitution for phenylalanine at residue Phe-129), and pST76A-SR/pOkaORF44K130A (with an alanine substitution for lysine at residue Lys-130), were generated from pST76A-SR/pOkaORF44 with a QuikChange Lightning multisite-directed mutagenesis kit using the primers listed in Table 1. Each mutated shuttle plasmid was transformed into DH10B harboring pOka-BACΔ44KMr, and *recA*-mediated allelic replacement was performed as described elsewhere (30) to generate pOka-BACORF44T128A, pOka-BACORF44F129A, and pOka-BACORF44K130A. The revertant BAC for the ORF44F129A mutant BAC, pOka-BACORF44F129ARev, was generated by *recA*-mediated allelic replacement using pST76A-SRORF44 transformed into pOka-BACORF44F129A-harboring DH10B.

All of the purified BACs were digested with BamHI or EcoRI to ensure that the expected DNA fragments were present, and the whole region for allelic replacement was sequenced to ensure that unexpected deletions or substitutions were not present.

Reconstitution of recombinant viruses and excision of the BAC cassette. MeWo cells or MeWoORF49 cells for rpOkaORF49M1L and rpOkaORF49-41AAAA44 seeded in one well of a 12-well plate were transfected with 3 μg of BAC DNA using Lipofectamine 2000 or X-treamGene HP (Roche Applied Science, Basel, Switzerland). After typical cytopathic effects (CPE) were seen in cells expressing green fluorescent protein (GFP), cell-free virus was prepared as described above and used to infect MeWo-Cre cells or pCX-Cre-neo-transfected MeWoORF49 cells for rpOkaORF49M1L and rpOkaORF49-41AAAA44 to excise the BAC cassette.

Immunoblotting, immunoprecipitation, and immunofluorescence. Immunoblotting, immunoprecipitation, and immunofluorescence were performed as described previously (30, 32) with slight modifications. The proteins in immunoblots were visualized by Chemi-Lumi One Super (Nacalai Tesque) in combination with LAS4000mini (GE Healthcare Bio-Sciences). Radioimmunoprecipitation assay (RIPA) lysis buffer (0.01 M Tris-HCl [pH 7.4], 0.15 M NaCl, 1% sodium deoxycholate, 1% Nonidet P-40, 0.1% SDS, 1 mM EDTA) supplemented with protease inhibitor cocktail (Sigma-Aldrich) was used for cell lysis, and the supernatants obtained by ultracentrifugation at 216,900 × *g* for 1 h at 4°C in a P50A3 rotor (CP80WX; Hitachi Koki) and precleared with protein G Sepharose 4 Fast Flow (GE Healthcare Bio-Sciences) were used for immunoblotting and immunoprecipitation. Immunofluorescence images were captured and analyzed by an FV1000D confocal microscope (Olympus, Tokyo, Japan).

***In vitro* binding assay.** To analyze the interaction of GST-ORF44 with ORF49, GST-ORF44, GST-ORF44F129A, or GST-ORF44P recombinant protein was expressed in and purified using BugBuster master mix (Merck Millipore, Darmstadt, Germany) from *E. coli* BL21 transformed with pGEX/ORF44, pGEX/ORF44F129A, or pGEX/ORF44P as described above. ORF49p was expressed in MeWo cells by transfection of CAG/ORF49 using Lipofectamine 2000 and solubilized as described above. GST-ORF44 recombinant protein was bound to glutathione Sepharose 4B (GE Healthcare Bio-Sciences) overnight at 4°C, washed with PBS three times, pelleted, and reacted with soluble ORF49p overnight at 4°C. The bead–GST-ORF44 recombinant protein–ORF49p complex was washed with RIPA lysis buffer three times, pelleted, suspended in SDS-PAGE sample buffer, boiled, and subjected to SDS-PAGE and immunoblotting as described above.

Protein identification by MS. MeWo cells were infected with pOka by cell-to-cell infection and lysed with RIPA lysis buffer as described above. The cell lysates from pOka- or mock-infected MeWo cells were precleared with protein G Sepharose and subjected to immunoprecipitation with anti-ORF49 Ab cross-linked protein G Sepharose. The immunoprecipitates were separated by SDS-PAGE and stained with a SilverQuest silver staining kit (Invitrogen). Protein bands were excised from the gel and digested with trypsin (sequencing grade; Promega, Madison, WI) according to published procedures (38). Nano-liquid chromatography-tandem mass spectrometry (nano-LC-MS/MS) analyses were performed on an LTQ-Orbitrap XL mass spectrometer (Thermo Fisher Scientific, Waltham, MA) equipped with a nano-electrospray ionization (nano-ESI) source (AMR, Tokyo, Japan) and coupled to a Paradigm MG4 pump (Michrom Bioresources, Auburn, CA) and autosampler (HTC PAL; CTC Analytics, Zwingen, Switzerland). A spray voltage of 1,800 V was applied. The peptide mixture was separated on a Magic C_{18} AQ column (100 μm by 150 mm, 3.0-μm particle size, 300 Å; Michrom Bioresources) with a flow rate of 500 nl/min. The linear gradient was as follows: 5% to 45% B in 30 min, 45% to 95% B in 0.1 min, 95% B for 2 min, and finally 5% B (solvent A = 0.1% formic acid in 2% acetonitrile, and B = 0.1% formic acid in 90% acetonitrile). Intact peptides were detected in the Orbitrap at a resolution of 60,000. For the LC-MS/MS analysis, six precursor ions were selected for subsequent MS/MS scans in a data-dependent acquisition mode following each full scan (m/z, 350 to 1,500). A lock mass function was used for the LTQ-Orbitrap to obtain constant mass accuracy during the gradient analysis. Peptides and proteins were identified by automated database searches using Proteome Discoverer v.1.1 (Thermo Fisher Scientific, Waltham, MA) against human entries or all entries of the Swiss-Prot protein database (version 3.26) with a precursor mass tolerance of 10 parts per million (ppm), a fragment ion mass tolerance of 0.8 Da, and strict trypsin specificity, allowing for up to two missed cleavages. Cysteine carbamidomethylation was set as a fixed modification, and methionine oxidation was allowed as a variable modification.

Plaque size and infectious-center assays for growth kinetics. To analyze the growth kinetics of the recombinant viruses, infectious-center assays were performed as described previously (6) with slight modifications. Briefly, 5×10^5 MeWo or MeWoORF49 cells were seeded on one well of a 12-well plate and inoculated with 50 PFU of cell-free virus per well. For the plaque size measurement, the infected cells were cultured for 7 days. For the infectious-center assay, infected cells were harvested at 24-h intervals and then titrated on newly prepared cells. The cells were fixed in 30% methanol and 70% acetone and stained with an anti-gE MAb (clone 9) and secondary ECL anti-mouse IgG horseradish peroxidase-linked whole antibody (GE Healthcare Bio-Sciences). The stain was developed with 3,3′,5,5′-tetramethylbenzidine-H (TMB-H) peroxidase substrate (Moss, Inc., Pasadena, MD). Images of the plaques were captured and traced, and the number of plaques was counted, or the plaque area was measured using ImageJ (http://rsbweb.nih.gov/ij/).

RESULTS

ORF49 functions in the efficient production of infectious progeny virus. To examine the mechanism of action of ORF49, we performed loss-of-function and gain-of-function analyses by generating an ORF49-defective virus, rpOkaORF49M1L, and its revertant virus, rpOkaORF49M1LRev, from the pOka-BACORF49M1L and pOka-BACORF49M1LRev genomes, respectively (Fig. 1A and C). In addition, the MeWoORF49 cell line was established to express ORF49 constitutively in MeWo cells in which the previous ORF49-defective virus, rpOkaΔ49, specifically showed an impaired growth phenotype (6), and gain-of-function analysis was performed by ORF49 *trans*-complementation assay.

None of the assayed viral proteins, including glycoprotein H (gH), ORF61 protein (ORF61p), ORF44p, and ORF49p, were detected in MeWo cells (Fig. 2A, lane 1). In MeWoORF49 cells, ORF49p was the only protein detected among the tested viral proteins (Fig. 2A, lane 2), and its expression level was comparable to that of ORF49p in rpOka-infected MeWo cells (Fig. 2A, lane 3). In rpOkaORF49M1L-infected cells, ORF49p was not detected in the infected MeWo cells (Fig. 2A, lane 4) or in the viral particles (Fig. 2C, lane 2), although gH and ORF61p were clearly expressed in infected cells (Fig. 2A, lane 4), as was gH in the viral particles (Fig. 2C, lane 2). The rpOkaORF49M1LRev line expressed all of the viral proteins tested (Fig. 2A, lane 5), similar to rpOka-infected MeWo cells (Fig. 2A, lane 3).

To confirm the ORF49-defective phenotype and perform gain-of function analysis, plaque formation was analyzed on MeWo and MeWoORF49 cells (Fig. 3A). Plaque sizes were similar between rpOka-infected MeWo and MeWoORF49 cells (Fig. 3A, lanes 1 and 2), indicating that the exogenous expression of ORF49 had neither positive nor negative effects on normal VZV infection. Similar to our previous results using rpOkaΔ49, rpOkaORF49M1L formed significantly smaller plaques on MeWo cells (Fig. 3A, lane 3) than on MeWoORF49 cells, and this reduction was recovered in the revertant virus infection in MeWo cells (Fig. 3A, lane 5) and completely rescued by the exogenous expression of ORF49 in MeWoORF49 cells (Fig. 3A, lane 4). Consistent with the plaque formation assay results, rpOkaORF49M1L propagated on MeWo cells showed slower growth than rpOka or rpOkaORF49M1LRev on MeWo or MeWoORF49 cells in an infectious-center assay, and the growth impairment of rpOkaORF49M1L was completely rescued by exogenous ORF49p in MeWoORF49 cells (Fig. 3B).

During the preparation of cell-free viruses, another strikingly different phenotype of the ORF49 defect was observed. As summarized in Table 2, the titer of cell-free virus or plaque size formed by the cell-free virus infection of rpOka was almost the same whether the virus was propagated on MeWo or MeWoORF49 cells or titrated on MeWo or MeWoORF49 cells, again indicating that the exogenous ORF49p had no effect on normal VZV infection. When rpOkaORF49M1L was propagated on MeWo cells, the titer of cell-free virus was 3 to 5% of that observed with propagation of MeWoORF49 cells, and the plaque size depended on the kind of cells used for titration but not on the kind used for propagation. In addition, the rpOkaORF49M1L particles isolated from MeWoORF49 cells contained abundant ORF49p (Fig. 2C, lane 3) and produced almost the same titer of cell-free virus as the parental virus but formed significantly smaller plaques on MeWo cells (Table 2). This gain-of-function analysis performed using the ORF49 *trans*-complementation system suggested that the incom-

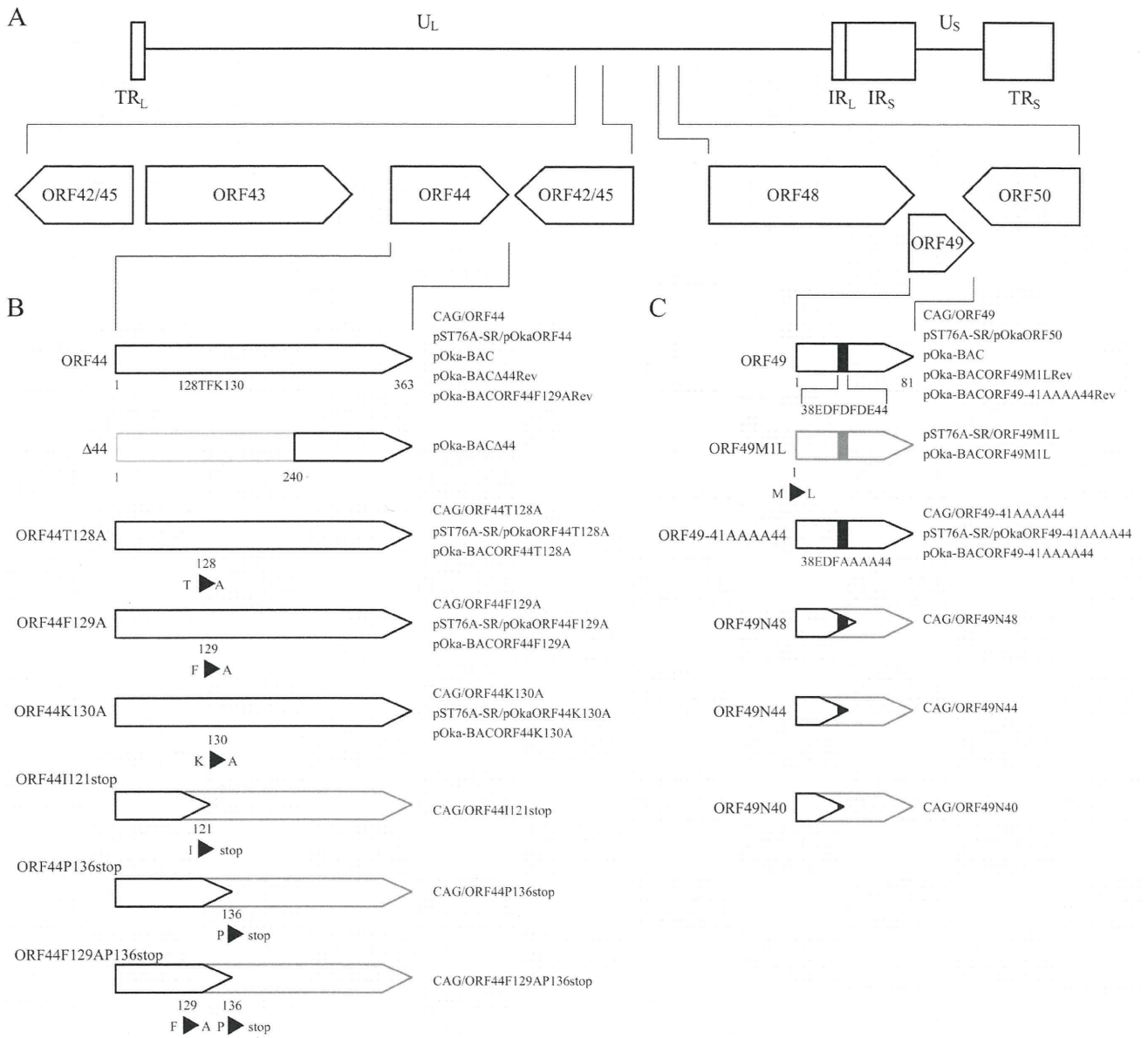

FIG 1 Schematics showing the plasmids and recombinant BAC genomes for ORF44 and ORF49. (A) Location of the ORF44 and ORF49 genes in the unique long region (U_L) segment of the genome of VZV strain pOka; terminal repeats (TR), unique short region (U_S), and internal repeats (IR) are indicated. (B) The wild type, deleted Δ44 region, and amino acid substitutions in ORF44p are shown. (C) The wild type, amino acid substitutions at the first methionine or the carboxyl-terminal half of the acidic cluster from amino acid positions 41 to 44, and the carboxyl-terminal truncations within ORF49p are shown. The acidic cluster is indicated as a black box. (B and C) Unexpressed regions of the mutant proteins are shown in gray outlined shapes. The names of relevant BACs, shuttle plasmids, and mammalian expression plasmids containing mutations are shown on the right.

ing ORF49p from the viral particles into the cells was not functional in any step and revealed that *de novo* ORF49p functioned in the production of infectious progeny viruses required for efficient propagation.

Furthermore, to examine the role of ORF49 in the production of infectious progeny viruses in detail, we redesigned our study on ORF49 to investigate its function by analyzing its binding partners.

Identification of the ORF44 protein as the binding partner for ORF49. ORF49p was immunoprecipitated from pOka- or mock-infected MeWo cells using an anti-ORF49 antibody (Ab), and the coimmunoprecipitating proteins were separated in a denaturing gel and visualized by silver staining (Fig. 4A). An approximately 36-kDa band was coimmunoprecipitated with the 13-kDa band corresponding to the ORF49p in pOka-infected MeWo cell lysates (Fig. 4A, lane 1). This 36-kDa band was identified as the ORF44 protein (ORF44p) of VZV by LC-MS/MS analysis (24.3% coverage of 363 amino acids).

ORF44p was specifically detected as a 36-kDa band in all recombinant VZV-infected MeWo cells, including rpOkaORF49M1L, by

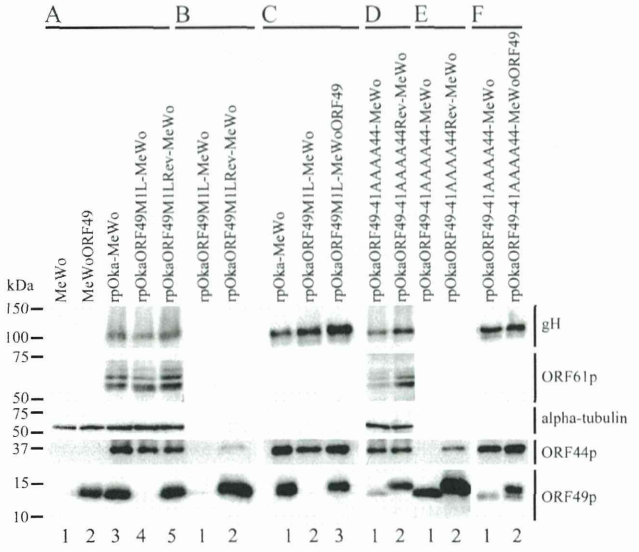

FIG 2 Expression and interaction of viral proteins during ORF49 mutant virus infection. (A) Proteins expressed in mock-infected MeWo cells (lane 1), mock-infected MeWoORF49 cells (lane 2), rpOka-infected MeWo cells (lane 3), rpOkaORF49M1L-infected MeWo cells (lane 4), and rpOkaORF49M1LRev-infected MeWo cells (lane 5) were visualized with Abs against gH, ORF61p, α-tubulin, ORF44p, and ORF49p. (B) The interaction between ORF44p and ORF49p was analyzed in rpOkaORF49M1L-infected cells (lane 1) and rpOkaORF49M1LRev-infected cells (lane 2). Immunoprecipitates obtained with an anti-ORF49 Ab from each type of virus-infected cells were electrophoretically separated and visualized using anti-ORF44 and anti-ORF49 Abs. (C) The viral proteins incorporated into virions from rpOka-infected MeWo cells (lane 1), rpOkaORF49M1L-infected MeWo cells (lane 2), and rpOkaORF49M1L-infected MeWoORF49 cells (lane 3) were visualized using Abs against gH, ORF61p, ORF44p, and ORF49p. (D) Proteins expressed in rpOkaORF49-41AAAA44-infected MeWo cells (lane 1) and rpOkaORF49-41AAAA44Rev-infected MeWo cells (lane 2) were visualized using Abs against gH, ORF61p, α-tubulin, ORF44p, and ORF49p. (E) The interaction between ORF44p and ORF49p was analyzed in rpOkaORF49-41AAAA44-infected cells (lane 1) and rpOkaORF49-41AAAA44Rev-infected cells (lane 2). Immunoprecipitates obtained using an anti-ORF49 Ab from each type of virus-infected cells were electrophoretically separated and visualized with anti-ORF44 and anti-ORF49 Abs. (F) The viral proteins incorporated into virions from rpOkaORF49-41AAAA44-infected MeWo cells (lane 1), and rpOka-ORF49-41AAAA44-infected MeWoORF49 cells (lane 2) were visualized with Abs against gH, ORF61p, ORF44p, and ORF49p.

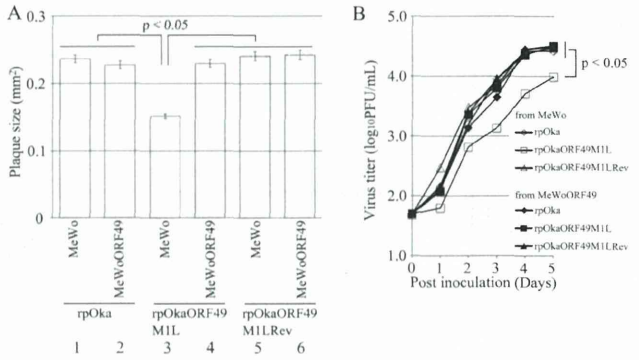

FIG 3 Growth properties of the ORF49M1L mutant virus in MeWo and MeWoORF49 cells. (A) Comparison of plaque sizes among recombinant viruses. MeWo cells or MeWoORF49 cells were infected with rpOka, rpOkaORF49M1L, or rpOkaORF49M1LRev (50 PFU/well) and cultured for 7 days. The infected cells were then stained with an anti-gE Ab, and the plaques were traced and measured by ImageJ software. Plaque size is shown with the standard error of the mean. Statistical significance was determined by Student's *t* test. (B) Growth kinetics of recombinant viruses in MeWo and MeWoORF49 cells. MeWo or MeWoORF49 cells were infected with rpOka, rpOkaORF49M1L, or rpOkaORF49M1LRev (50 PFU/well), harvested at the indicated times, serially diluted, added to newly prepared MeWo cells, and cultured for 5 days. The plaques were stained with an anti-gE Ab and counted. Each point represents the mean titer for two wells of one experiment. The experiments were performed twice independently. Statistical significance was determined by Student's *t* test.

immunoblotting with an anti-ORF44 Ab (Fig. 2A, lanes 3, 4, and 5). ORF44p was coimmunoprecipitated with ORF49p only in cells infected with the wild-type virus, rpOka, or rpOkaORF49M1LRev (data not shown) (Fig. 2B, lane 2) but not in the absence of ORF49p, as seen in rpOkaORF49M1L infection (Fig. 2B, lane 1). Thus, the interaction of ORF44p and ORF49p was specific and conserved in VZV.

ORF44 is essential for viral growth in cell culture. Because ORF49 is completely dispensable for viral reconstitution and propagation in MRC-5 cells, and the interaction between ORF44p and ORF49p was confirmed, we predicted that the ORF44 deletion mutant would be viable at least in MRC-5 cells, despite the fact that loss-of-function analysis showed that it is essential in MeWo cells (5). The ORF44 deletion mutant virus could not be reconstituted from pOka-BACΔ44 (Fig. 1B) in either MeWo cells or MRC-5 cells; however, the revertant virus of pOka-BACΔ44 reconstituted from the pOka-BACΔ44Rev genome (Fig. 1B) showed almost the same plaque size and growth as the parental virus, rpOka, in MeWo cells (data not shown). These findings confirmed that ORF44 is essential for VZV growth in cell culture even in MRC-5 cells.

ORF44p binds to and depends on ORF49p for its accumulation on the TGN in coexpressing cells and infection. When ORF44p was expressed alone by CAG/ORF44 transfection, it was dispersed throughout the cytoplasm and did not localize to the TGN (Fig. 5A). When ORF49p was expressed alone, it was predominantly localized to the juxtanuclear region with TGN46 (Fig. 5B), as reported previously (6). In cells coexpressing ORF44 and ORF49, ORF44p accumulated on the TGN with ORF49p (Fig. 5C), suggesting that the complex formation between ORF44p and ORF49p required no other viral factors and that it functioned in the accumulation of the ORF44p on the TGN. The expression of and interaction

TABLE 2 Comparison of cell-free virus titer and plaque formation

Virus	Cells for: Propagation	Titration	Titer (PFU/ml)[a]	Mean (SE) plaque size, mm²[b]
rpOka	MeWo	MeWo	2.3×10^3	0.232 (0.00891)
	MeWo	MeWoORF49	4.1×10^3	0.225 (0.00854)
	MeWoORF49	MeWo	4.0×10^3	0.232 (0.00911)
	MeWoORF49	MeWoORF49	1.3×10^3	0.206 (0.00828)
rpOkaORF49M1L	MeWo	MeWo	1.5×10^2	0.161 (0.00601)
	MeWo	MeWoORF49	1.7×10^2	0.235 (0.01319)
	MeWoORF49	MeWo	4.0×10^3	0.147 (0.00534)
	MeWoORF49	MeWoORF49	6.3×10^3	0.228 (0.01474)
rpOkaORF49-41AAAA44	MeWo	MeWo	1.2×10^2	0.141 (0.00726)
	MeWo	MeWoORF49	1.3×10^2	0.212 (0.00669)
	MeWoORF49	MeWo	2.1×10^3	0.149 (0.00796)
	MeWoORF49	MeWoORF49	4.7×10^3	0.227 (0.00740)

[a] Titers of cell free viruses are shown from one experiment performed in duplicate.
[b] Plaque sizes are shown as means (standard errors [SE]) from one experiment performed in duplicate.

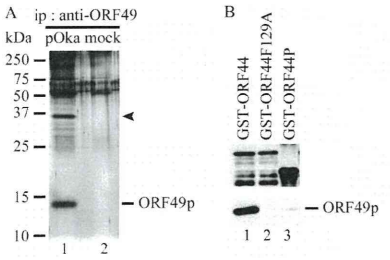

FIG 4 Identification of ORF44p as the binding partner of ORF49p by proteomic analysis and their *in vitro* binding assay. (A) pOka-infected MeWo cells expanded by cell-to-cell spread with full CPE at 2 to 3 days postinfection were lysed with RIPA buffer, and the binding molecules were coimmunoprecipitated with ORF49p using an anti-ORF49 Ab (lane 1). Mock-infected MeWo cells were used as a negative control (lane 2). The immunoprecipitates (ip) were electrophoretically separated and visualized by silver staining. (B) ORF49p expressed in and purified from MeWo cells was incubated with purified GST-ORF44 (lane 1), GST-ORF44F129A (lane 2), or GST-ORF44P (lane 3). Bound proteins were electrophoretically separated and visualized by anti-GST Abs (upper panel) and anti-ORF49 Abs (lower panel).

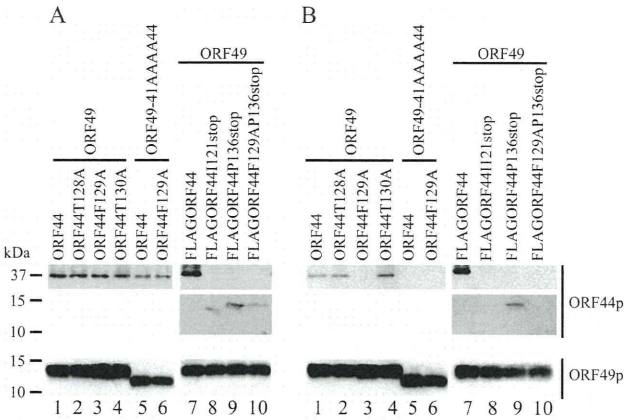

FIG 6 Expression and interaction of ORF44p and ORF49p in cotransfected cells. MeWo cells were cotransfected with CAG/ORF49 (lanes 1 to 4 and 7 to 10) or CAG/ORF49-41AAAA44 (lanes 5 and 6) and CAG/ORF44 (lanes 1 and 5), CAG/ORF44T128A (lane 2), CAG/ORF44F129A (lanes 3 and 6), CAG/ORF44K130A (lane 4), CAG/FLAGORF44 (lane 7), CAG/FLAGORF44I121stop (lane 8), CAG/FLAGORF44P136stop (lane 9), or CAG/FLAGORF44F129AP136stop (lane 10) (A and B). Protein expression was visualized with anti-ORF44p and anti-ORF49p antibodies (A), and proteins immunoprecipitated by anti-ORF49 Ab from cotransfected cells were electrophoretically separated and visualized using anti-ORF44 and anti-ORF49 Abs (B).

between ORF44p and ORF49p were confirmed by immunoblotting with the corresponding Abs and immunoprecipitation with anti-ORF49 Ab followed by immunoblotting with each Ab (Fig. 6A, lane 1, and B, lane 1, respectively). In rpOkaORF49M1LRev-infected MeWo cells, in spite of the broadly diffuse pattern seen for ORF44p, it appeared to accumulate on the TGN with ORF49p (Fig. 7B), as was seen in coexpressing cells (Fig. 5C), and this pattern was also observed in cells infected with rpOka (data not shown). In rpOkaORF49M1L-infected cells, ORF44p was dispersed as in cells expressing ORF44 alone and was not accumulated on the TGN (Fig. 7A), again indicating that the accumulation of ORF44p on the TGN depended on ORF49p and required no other viral factors.

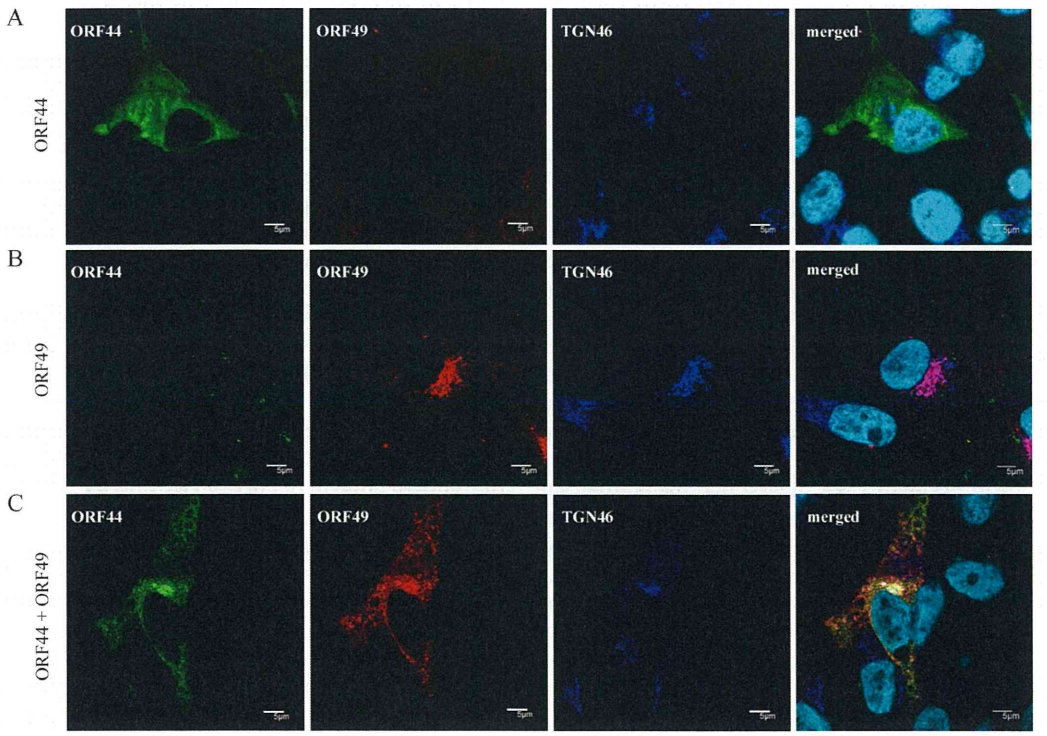

FIG 5 Localization of ORF44p and ORF49p in transiently transfected MeWo cells. MeWo cells were transfected with CAG/ORF44 (A) or CAG/ORF49 (B) or cotransfected with CAG/ORF44 and CAG/ORF49 (C). Cells were fixed at 48 h posttransfection and triple labeled for ORF44p (green), ORF49p (red), and TGN46 (blue). Nuclei were stained with Hoechst 33342 (cyan). Scale bars, 5 μm.

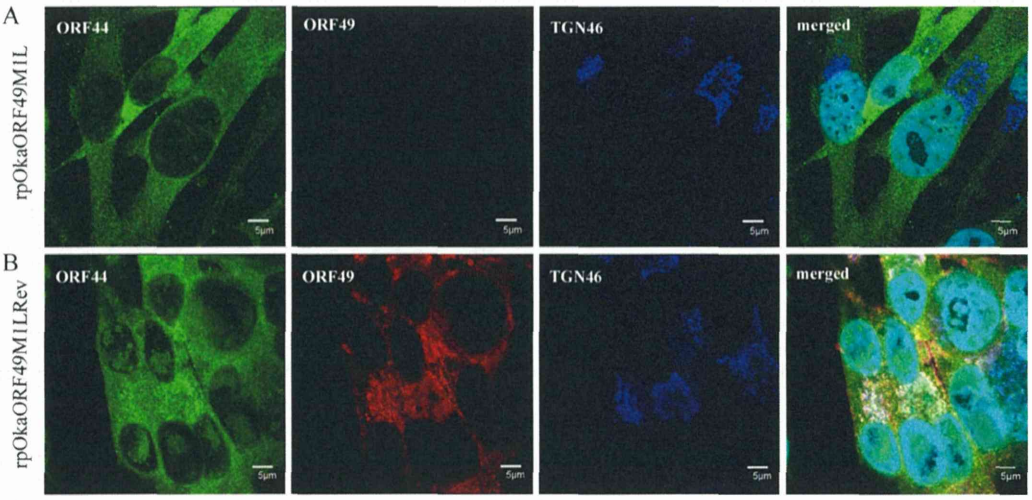

FIG 7 Localization of ORF44p and ORF49p in rpOkaORF49M1L-infected MeWo cells. rpOkaORF49M1L-infected (A) and rpOkaORF49M1LRev-infected (B) MeWo cells were fixed at 48 hpi and triple labeled for ORF44p (green), ORF49p (red), and TGN46 (blue). Nuclei were stained with Hoechst 33342 (cyan). Scale bars, 5 μm.

The phenylalanine at amino acid position 129 of ORF44p functions in the conserved interaction and is essential for VZV infection. In the process of ORF44 cloning, one mutant showed a T-to-C substitution at nt 385, which led to a phenylalanine-to-serine transition at aa 129 (F129S). In cells coexpressing ORF44F129Sp and ORF49p, ORF44F129Sp did not accumulate on the TGN and was not coimmunoprecipitated with ORF49p (data not shown).

To examine whether 129F functions specifically in the conserved interaction in VZV, alanine scanning was performed around 129F (Fig. 1B). ORF44T128Ap, ORF44F129Ap, and ORF44K130Ap showed similar distributions, and none of these mutants localized to the TGN when expressed alone (data not shown), as observed in cells expressing ORF44p alone (Fig. 5A). Coexpression of ORF44T128Ap and ORF44K130Ap with ORF49p (Fig. 8A and C, respectively) resulted in their colocalization with ORF49p at the TGN, as observed in cells coexpressing ORF44p and ORF49p (Fig. 5C). In contrast, ORF44F129Ap was dispersed throughout the cytoplasm and failed to accumulate on the TGN, even when coexpressed with ORF49p (Fig. 8B). The levels of expression of ORF44T128Ap, ORF44F129Ap, and ORF44K130Ap were almost equal (Fig. 6A, lanes 2, 3, and 4, respectively), and ORF44T128Ap and ORF44K130Ap were coimmunoprecipitated with ORF49p (Fig. 6B, lanes 2 and 4, respectively), whereas ORF44F129Ap was not coimmunoprecipitated with ORF49p (Fig. 6B, lane 3).

The results for F129S and F129A suggest that the binding site for ORF49p might reside in an N-terminal domain, as was recently reported for the pUL16 of HSV-1 (26). Therefore, stop codons were inserted at positions to either side of codon 129F (i.e., at I121stop and P136stop). In addition, a construct containing both the F129A and P136stop mutations was made (Fig. 1B). All three mutants were expressed at their predicted size (Fig. 6A, lanes 8, 9, and 10), and only the ORF44P136stop protein was coimmunoprecipitated with ORF49p (Fig. 6B, lane 9), whereas the ORF44I121stop and ORF44F129AP136stop proteins were not (Fig. 6B, lanes 8 and 10, respectively). Consistent with this, only the ORF44P136stop protein accumulated on the TGN with ORF49p (Fig. 8E), and the other two mutants did not (Fig. 8D and F), despite the diffused cytoplasmic localization of all mutants if expressed alone (data not shown). These results show that the binding site for ORF49p resides in the first third of ORF44p and that 129F plays a critical role in binding, either directly or indirectly. Furthermore, in GST-pulldown assays using GST-ORF44 (corresponding to aa 2 to 363), GST-ORF44F129A (aa 2 to 363 with F129A mutation), and GST-ORF44P (aa 180 to 363), only GST-ORF44 pulled down ORF49p expressed in and purified from MeWo cells (Fig. 4B), suggesting that there may not be a binding site within the C-terminal half of ORF44p; however, other C-terminal constructs have not been tested in this or other assays.

To analyze the impact of the 129F mutation in the context of infection, pOka-BACORF44T128A, pOka-BACORF44F129A, pOka-BACORF44K130A, and the revertant BAC for pOka-BACORF44F129A, pOka-BACORF44F129ARev, were generated (Fig. 1B). With the exception of the ORF44F129A mutant, the reconstitution of each virus with a mutation around 129F and of the revertant virus for the F129A mutant was successful, and all of the reconstituted viruses showed similar growth to rpOka (data not shown), suggesting that 129F of ORF44p may play a central role in the function of ORF44p in VZV infection, which occurs through its interaction with ORF49p.

The carboxyl-terminal half of the acidic cluster of ORF49p is required for the conserved interaction with ORF44p. To map the binding domain of ORF49p for ORF44p using the accumulation of ORF44p as an indicator of the interaction, we generated a series of carboxyl-terminal-truncated mutants of ORF49p (Fig. 1C). The coexpression of ORF44p and ORF49N48p or ORF49N44p resulted in the accumulation of ORF44p at the juxtanuclear region with TGN46 and the mutant ORF49p (Fig. 9A and B). In contrast, ORF44p never colocalized with ORF49N40p (Fig. 9C) and was dispersed in the cytoplasm, as when it was expressed alone (Fig. 5A). These results suggested that the ORF44p-binding domain in ORF49p may be located between the aspartate at aa 41 and glutamate at aa 44, which is in the carboxyl-terminal half of the conserved acidic cluster (Fig. 1C) in the ORF49 homologs.

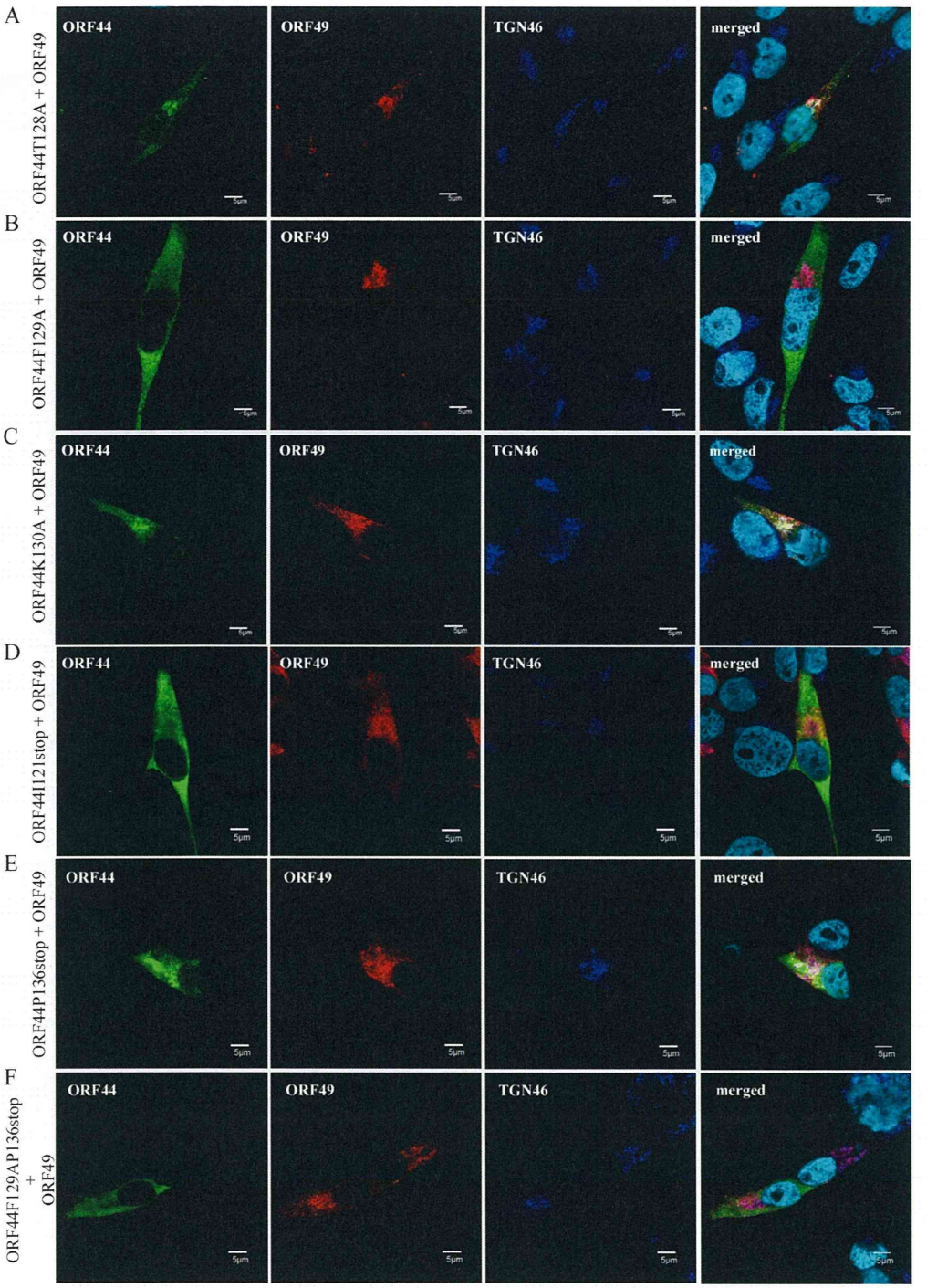

FIG 8 Localization and accumulation of ORF44 mutant proteins in MeWo cells expressing ORF49p. MeWo cells were cotransfected with CAG/ORF49 and CAG/ORF44T128A (A), CAG/ORF44F129A (B), CAG/ORF44K130A (C), CAG/FLAGORF44I121stop (D), CAG/FLAGORF44P136stop (E), or CAG/FLAGORF44F129AP136stop (F). Cells were fixed at 48 h posttransfection and triple labeled for ORF44 (green), ORF49 (red), and TGN46 (blue). Nuclei were stained with Hoechst 33342 (cyan). Scale bars, 5 μm.

To confirm the specificity of the ORF44p and ORF49p interaction while avoiding (although not excluding) nonspecific effects on the function of ORF49p resulting from the destruction of the ORF49p backbone, the four residues (41DFDE44) identified as the candidate ORF44p-binding motif were replaced by alanine, resulting in ORF49-41AAAA44p (Fig. 1C). As shown in Fig. 9D, ORF49-41AAAA44p targeted the TGN, similar to ORF49p (Fig. 5B), but it was unable to accumulate ORF44p on the TGN (Fig. 9E).